

---

# HYPERBOLIC PHONON-PLASMON POLARITONS IN A hBN-GRAPHENE VAN DER WAALS STRUCTURE

---

A PREPRINT

✉ **Yu. V. Bludov**<sup>\*1</sup>, ✉ **D. A. Bahamon**<sup>2,3</sup>, ✉ **N. M. R. Peres**<sup>1,4,5</sup>, and ✉ **C. J. S. de Matos**<sup>2,3</sup>

<sup>1</sup>Centro de Física (CF-UM-UP) e Departamento de Física, Universidade do Minho, PT-4710-057, Braga, Portugal

<sup>2</sup>School of Engineering, Mackenzie Presbyterian University, São Paulo 01302-907, Brazil

<sup>3</sup>MackGraphe-Graphene and Nanomaterials Research Institute, Mackenzie Presbyterian Institute, São Paulo 01302-907, Brazil

<sup>4</sup>International Iberian Nanotechnology Laboratory (INL), Av. Mestre José Veiga, 4715-330 Braga, Portugal

<sup>5</sup>POLIMA—Center for Polariton-driven Light–Matter Interactions, University of Southern Denmark, Campusvej 55, DK-5230 Odense M, Denmark

## ABSTRACT

In this paper a thorough theoretical study of a new class of collective excitations, dubbed hyperbolic surface phonon plasmon polaritons, is performed. This new type of light-matter excitations are shown to have unique properties that allows to explore them both as the basis of ultra-sensitive devices to the dielectric nature of its surroundings. The system is a van der Waals heterostructure – a layered metamaterial, composed of different 2D materials in direct contact one with another, namely graphene ribbons and hexagonal boron nitride slabs of nanometric size. In the paper we discuss the spectrum of these new class of excitations, the associated electromagnetic fields, the sensitivity to the dielectric function of its surroundings, and the absorption spectrum. All this is accomplished using an analytical model that considerably diminishes the computational burden, as well as elucidates the underling physical mechanism of the excitations supported by the device.

## 1 Introduction

In solid state structures electromagnetic radiation can be effectively coupled to the mechanical oscillations of charges, forming hybrid modes, known as polaritons[1]. More specifically, electromagnetic radiation can be coupled to free charge oscillations in metals (plasmons)[2, 3, 4], to phonons in dielectrics[5], to excitons in semiconductor[6], or to the spin oscillations in magnetic materials (magnons)[7, 8]. The resulting modes are known as plasmon-polariton, phonon-polariton, exciton-polariton, and magnon-polariton, respectively. A general tendency for the miniaturization of electronic and photonic components attracted researcher’s interest to the investigation of the two-dimensional solid-state structures, which are also able to sustain polaritons with longer mean free path, if compared to the bulk structures. In detail, surface plasmon-polaritons[9, 10, 11], phonon-polaritons[12] and exciton-polaritons[13] can exist in graphene, hexagonal Boron Nitride (hBN), and transition metal dichalcogenetes (TMDs), correspondingly. At the same time, surface plasmon-polaritons in graphene exist in the THz and far-infrared spectral range[14], i.e. in the domain of typical frequencies of optical phonons in dielectrics[15, 16, 17, 18, 19, 20]. The latter fact allows the interaction between plasmons, optical phonons and electromagnetic radiation, which leads to the formation of hybrid modes, known as surface phonon-plasmon polaritons[21, 22, 23]. Experimentally these hybrid modes were observed in the graphene, deposited on top of SiO<sub>2</sub>[24], SiC[25, 23] or hBN[26] substrates. When the thickness of the hBN layer is finite, the spectrum of eigenmodes consists of infinite number of waveguide modes[27, 28, 29, 30], which exists in the upper and lower restrahlen bands (RBs), where, respectively, longitudinal or transversal component of the dielectric tensor is negative.

Since the modes mentioned above are surface modes (whose in-plane wavevector is bigger than that of bulk electromagnetic wave in vacuum), they can not be excited directly by an external wave, impinging on the layered structure.

---

\*bludov@fisica.uminho.pt

One of the possibilities to overcome this wavevector mismatch is to use the periodically patterned structure, where the excitation of hybrid mode takes place, when the wavevector of one of diffraction harmonics coincide with wavevector of eigenmode. Among other possibilities, like nanoresonators[31, 32, 33, 34, 35], disks[36, 37], nanostructured substrate [38, 39, 40, 41], or periodically patterned layer on top of graphene [42, 43], a graphene monolayer patterned in form of nanoribbons[44, 45, 46, 47, 48, 49, 50] attracts a special attention owing to both relatively easy sample preparation and the possibility to theoretically model it, applying simple analytical methods[51, 52, 53]. Another important application of an array of graphene nanoribbons is their possibility to be used in sensing [54, 55, 56, 57, 58, 59, 60, 61, 62, 63, 64, 65]. Since in the sensing by means of graphene nanoribbons the analyte is arranged in the vicinity of graphene strips, where field of SPPs is maximal, phenomena in these structure have strong similarity with surface-enhanced infrared absorption (SEIRA), where weak light matter interaction is overcome by putting analyte into the hot spots of electromagnetic field[66, 67, 68]. In this paper a diffraction grating is realized by periodic patterning the graphene. Thus, a graphene monolayer [located in  $xy$ -plane at  $z = 0$ , see Fig. 1(a)] is considered to be patterned into an array of strips with period  $D$ . Each individual strip is supposed to be infinite in the  $y$ -direction and of finite width  $W$  in the  $x$ -direction [see Fig. 1(a)], arranged in the spatial interval  $-W/2 + lD \leq x \leq W/2 + lD$ , where  $l$  is the strip's number. The array of graphene nanostrips is cladded by two hBN layers of thicknesses  $d_b$  and  $d_t$  (for bottom and top layers, respectively). Since this graphene-hBN hybrid structure is supposed to be used in the plasmonic sensing application, the top hBN layer is considered to be covered with an analyte, which is modelled by the dielectric layer of thickness  $d_a$  and refractive index  $n_a$ , arranged in spatial domain  $z_2 = -d_a - d_t \leq z \leq z_3 = -d_t$ . The resulting layered structure is supposed to be truncated from both sides by vacuum/air (for at  $z > z_5 = d_b$  and  $z < z_2 = -d_a - d_t$ ). We consider, that an external plane electromagnetic wave impinges on the analyte from vacuum side.

## 2 Diffraction of an electromagnetic wave by the periodic structure

The fact that surface phonon-plasmon-polaritons are p-polarized waves (where the direction of the magnetic field is perpendicular to the direction of propagation), and the uniformity of the structures in Fig. 1 along the  $y$ -direction, allows the description of their electromagnetic properties by means of Maxwell's equations, which involves the  $y$ -component of magnetic field,  $\mathbf{H} = (0, H_y, 0)$ , as well as  $x$ - and  $z$ -components of the electric field,  $\mathbf{E} = (E_x, 0, E_z)$ . Considering the electromagnetic field time-dependency as  $\mathbf{E}, \mathbf{H} \sim \exp(-i\omega t)$ , respective Maxwell's equations can be written in Gaussian units as

$$\frac{\partial E_x^{(\alpha)}}{\partial z} - \frac{\partial E_z^{(\alpha)}}{\partial x} = \frac{i\omega}{c} H_y^{(\alpha)}, \quad (1)$$

$$-\frac{\partial H_y^{(\alpha)}}{\partial z} = -\frac{i\omega}{c} \varepsilon_{xx}^{(\alpha)} E_x^{(\alpha)}, \quad (2)$$

$$\frac{\partial H_y^{(\alpha)}}{\partial x} = -\frac{i\omega}{c} \varepsilon_{zz}^{(\alpha)} E_z^{(\alpha)}. \quad (3)$$

where  $\omega$  is the wave cyclic frequency,  $c$  is the velocity of light in vacuum. Superscript  $\alpha$  corresponds to the electromagnetic fields in different dielectric layers, characterized by the dielectric permittivity tensor, involving diagonal components only, i.e.  $\varepsilon_{xx}^{(\alpha)}$  and  $\varepsilon_{zz}^{(\alpha)}$ .

Taking into account normal incidence of external electromagnetic wave, and, as a consequence, independence of electromagnetic field upon  $x$ -coordinate, the solution of Maxwell's equations (1)–(3) can be obtained in the form of a Fourier-Floquet series with respect to cosine-like functions, which even symmetries coincide with that of incident wave. Sine-like harmonics can not be excited by normally incident wave owing to their odd symmetries. In the semi-infinite vacuum/air region  $z < z_2 = -d_a - d_t$  the solution of Maxwell's equations can be represented as a superposition of forward-propagating (in  $z$ -direction) incident wave with amplitude of magnetic field  $H_y^{(i)}$ , and infinite number of backward-propagating spatial harmonics of reflected field with magnetic-field amplitudes  $H_{y||m}^{(r)}$ . In the matrix form this type of solution can be represented as

$$\begin{pmatrix} H_y^{(1)}(x, z) \\ E_x^{(1)}(x, z) \end{pmatrix} = \sum_{m=0}^{\infty} \cos \left[ \frac{2\pi m}{D} x \right] \hat{F}_m \quad (4)$$

$$\times \begin{pmatrix} H_y^{(i)} \delta_{m,0} \exp[ip_m(z - z_2)] \\ H_{y||m}^{(r)} \exp[-ip_m(z - z_2)] \end{pmatrix},$$

where

$$\hat{F}_m = \begin{pmatrix} 1 & 1 \\ \frac{cp_m}{\omega} & -\frac{cp_m}{\omega} \end{pmatrix}$$

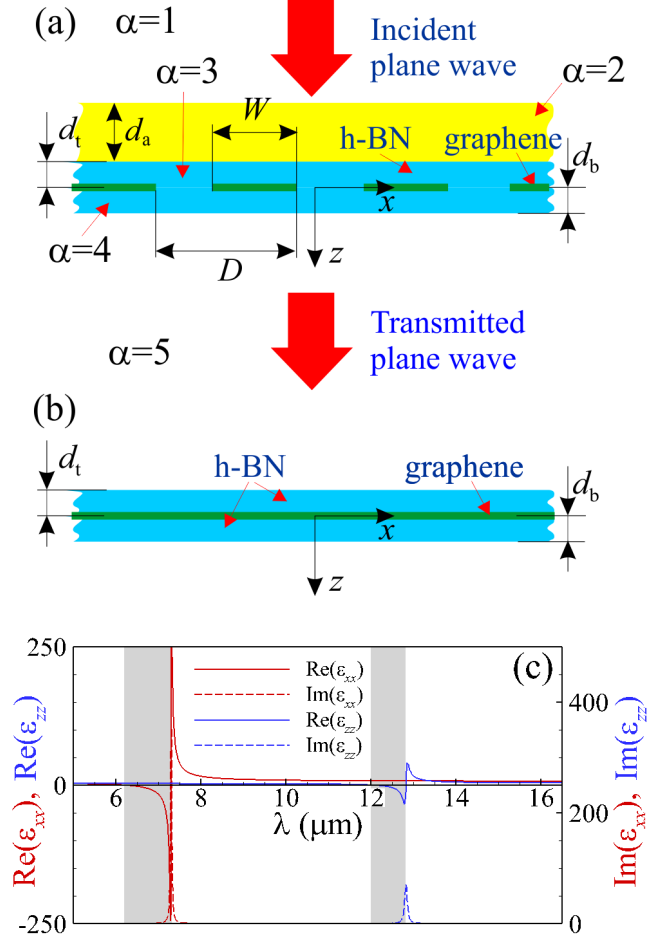


Figure 1: Layered structures, able to sustain surface phonon-plasmon polaritons: (a) periodic array of graphene nanostrips cladded by two layers of h-BN (with thicknesses of top and bottom layers  $d_t$  and  $d_b$ , respectively), and covered with analyte layer of finite thickness; (b) Uniform graphene monolayer, cladded between two hBN layers; (c) Real (left axis) and imaginary (right axis) parts of the hBN dielectric tensor [see Eqs. (9) and (10)]. Reststrahlen bands are shadowed by grey color.

is the field matrix,

$$p_m = \sqrt{\left(\frac{\omega}{c}\right)^2 - \left(\frac{2\pi m}{D}\right)^2}$$

is the out-of-plane wavevector component of the  $m$ th harmonics in vacuum (the respective in-plane component is equal to  $2\pi m/D$ ), and  $\delta_{m,m'}$  is Kronecker delta. For the other semi-infinite vacuum/air region,  $z > z_5 = d_b$ , the solution of Maxwell's equation includes forward-propagating harmonics of transmitted wave only, i.e.

$$\begin{pmatrix} H_y^{(5)}(x, z) \\ E_x^{(5)}(x, z) \end{pmatrix} = \sum_{m=0}^{\infty} \cos\left[\frac{2\pi m}{D}x\right] \hat{F}_m \quad (5)$$

$$\times \begin{pmatrix} H_{y||m}^{(t)} \exp[ip_m(z - z_5)] \\ 0 \end{pmatrix}.$$

Here zero in the second line means absence of the backward-propagating harmonics, mentioned above.

In the semi-infinite regions, occupied by air/vacuum, solutions of Maxwell's equations [see Eqs.(4) and (5)] are parametrized by the amplitudes of the magnetic field of forward- and backward-propagating harmonics. Inside the layers of finite thickness the solution of Maxwell's equations will be parametrized in different manner – by the

amplitudes of the electric- and magnetic fields' tangential components,  $e_{x||m}^{(\alpha)}$  and  $h_{y||m}^{(\alpha)}$ , at one of the layer boundaries. The spatial dependence of the electromagnetic field inside the dielectric slab is determined by the transfer-matrix

$$\hat{Q}_m^{(\alpha)}(z) = \begin{pmatrix} \cos[q_m^{(\alpha)} z] & \frac{i\omega\varepsilon_{xx}^{(\alpha)}(\omega)}{cq_m^{(\alpha)}} \sin[q_m^{(\alpha)} z] \\ \frac{icp_m^{(\alpha)}}{\omega\varepsilon_{xx}^{(\alpha)}(\omega)} \sin[q_m^{(\alpha)} z] & \cos[q_m^{(\alpha)} z] \end{pmatrix}, \quad (6)$$

where in the case of anisotropic medium the out-of-plane component of wavevector is represented as  $q_m^{(\alpha)} = \sqrt{(\frac{\omega}{c})^2 \varepsilon_{xx}^{(\alpha)}(\omega) - (\frac{2\pi m}{D})^2 \varepsilon_{xx}^{(\alpha)}(\omega) / \varepsilon_{zz}^{(\alpha)}(\omega)}$ . Inside the top ( $\alpha = 3$ ) and bottom ( $\alpha = 4$ ) hBN layers, the spatial dependence of total electromagnetic field have the form

$$\begin{pmatrix} H_y^{(3)}(x, z) \\ E_x^{(3)}(x, z) \end{pmatrix} = \sum_{m=0}^{\infty} \cos\left[\frac{2\pi m}{D}x\right] \times \hat{Q}_m^{(3)}(z + d_t) \begin{pmatrix} h_{y||m}^{(3)}(z_3) \\ e_{x||m}^{(3)}(z_3) \end{pmatrix}, \quad (7)$$

$$\begin{pmatrix} H_y^{(4)}(x, z) \\ E_x^{(4)}(x, z) \end{pmatrix} = \sum_{m=0}^{\infty} \cos\left[\frac{2\pi m}{D}x\right] \times \hat{Q}_m^{(4)}(z - d_b) \begin{pmatrix} h_{y||m}^{(4)}(z_5) \\ e_{x||m}^{(4)}(z_5) \end{pmatrix}. \quad (8)$$

Here the components of hBN dielectric permeability tensor are[69]

$$\begin{aligned} \varepsilon_{xx}^{(3)}(\omega) = \varepsilon_{xx}^{(4)}(\omega) = \varepsilon_{xx}(\infty) \\ \times \left( 1 + \frac{(\omega_{xx}^{(LO)})^2 - (\omega_{xx}^{(TO)})^2}{(\omega_{xx}^{(TO)})^2 - \omega^2 - i\omega\Gamma_{xx}^{(TO)}} \right), \end{aligned} \quad (9)$$

$$\begin{aligned} \varepsilon_{zz}^{(3)}(\omega) = \varepsilon_{zz}^{(4)}(\omega) = \varepsilon_{zz}(\infty) \\ \times \left( 1 + \frac{(\omega_{zz}^{(LO)})^2 - (\omega_{zz}^{(TO)})^2}{(\omega_{zz}^{(TO)})^2 - \omega^2 - i\omega\Gamma_{zz}^{(TO)}} \right), \end{aligned} \quad (10)$$

with parameters  $\omega_{xx}^{(TO)} = 1370 \text{ cm}^{-1}$ ,  $\omega_{xx}^{(LO)} = 1610 \text{ cm}^{-1}$ ,  $\Gamma_{xx}^{(TO)} = 5 \text{ cm}^{-1}$ ,  $\omega_{zz}^{(TO)} = 780 \text{ cm}^{-1}$ ,  $\omega_{zz}^{(LO)} = 830 \text{ cm}^{-1}$ ,  $\Gamma_{zz}^{(TO)} = 4 \text{ cm}^{-1}$ ,  $\varepsilon_{xx}(\infty) = 4.87$ ,  $\varepsilon_{zz}(\infty) = 2.95$ . The respective dependence of hBN dielectric permeability tensor components upon vacuum wavelength  $\lambda$  are depicted in Fig. 1(c). The analyte medium ( $\alpha = 2$ ) is assumed to be isotropic throughout this paper, thus its dielectric tensor components in Eq. (6) are assumed to be  $\varepsilon_{xx}^{(2)}(\omega) = \varepsilon_{zz}^{(2)}(\omega) = n_a^2$ . The respective electromagnetic fields inside the spatial domain, occupied by the analyte layer, are

$$\begin{pmatrix} H_y^{(2)}(x, z) \\ E_x^{(2)}(x, z) \end{pmatrix} = \sum_{m=0}^{\infty} \cos\left[\frac{2\pi m}{D}x\right] \times \hat{Q}_m^{(2)}(z - z_2) \begin{pmatrix} h_{y||m}^{(2)}(z_2) \\ e_{x||m}^{(2)}(z_2) \end{pmatrix}. \quad (11)$$

Since the boundary conditions at interfaces  $z = z_2, z_3, z_5$  can be expressed as the continuity of the tangential components of the electromagnetic fields, i.e.  $\left(H_y^{(\alpha-1)}(x, z_\alpha), E_x^{(\alpha-1)}(x, z_\alpha)\right)^T = \left(H_y^{(\alpha)}(x, z_\alpha), E_x^{(\alpha)}(x, z_\alpha)\right)^T$ , the electromagnetic fields at both sides of graphene layer (arranged at  $z = z_4 = 0$ ) can be obtained by the multiplication of field- and transfer matrices. Being expressed through amplitudes of the magnetic field in the semi-infinite media, the

respective fields take the form

$$\begin{pmatrix} H_y^{(3)}(x, 0) \\ E_x^{(3)}(x, 0) \end{pmatrix} = \sum_{m=0}^{\infty} \cos \left[ \frac{2\pi m}{D} x \right] \hat{F}_m^{(-, tot)} \times \begin{pmatrix} H_y^{(i)} \delta_{m,0} \\ H_{y||m}^{(r)} \end{pmatrix}, \quad (12)$$

$$\begin{pmatrix} H_y^{(4)}(x, 0) \\ E_x^{(4)}(x, 0) \end{pmatrix} = \sum_{m=0}^{\infty} \cos \left[ \frac{2\pi m}{D} x \right] \hat{F}_m^{(+, tot)} \times \begin{pmatrix} H_{y||m}^{(t)} \\ 0 \end{pmatrix}, \quad (13)$$

where  $\hat{F}_m^{(-, tot)} = \hat{Q}_m^{(3)}(d_t) \hat{Q}_m^{(2)}(d_a) \hat{F}_m$ ,  $\hat{F}_m^{(+, tot)} = \hat{Q}_m^{(4)}(-d_b) \hat{F}_m$  are total field matrices above and below the graphene layer. The boundary condition across the graphene has a different form: the electric field's tangential component is continuous across the graphene,  $E_x^{(4)}(x, 0) = E_x^{(3)}(x, 0)$ , while magnetic field is discontinuous owing to the presence of currents in graphene,

$$H_y^{(4)}(x, 0) - H_y^{(3)}(x, 0) = -(4\pi/c) j_x(x). \quad (14)$$

In the case of nanostrips array the current in graphene can be approximated by square-root-like function [51]

$$j_x(x) = \sum_{l=-\infty}^{\infty} j_x(0) \Theta \left( \frac{W}{2} - |x - lD| \right) \times \sqrt{1 - \frac{4}{W^2} (x - lD)^2}, \quad (15)$$

where  $\Theta(x)$  is the Heaviside step-like function. In this expression we applied Bloch theorem  $j_x(lD) = j_x(0)$  and supposed, that at the edges of each individual strip the current is zero,  $j_x(\pm W/2 + lD) \equiv 0$ , and there are no currents between strips. Substituting magnetic fields from Eqs. (12), (13), as well as current (15) into boundary condition (14), we have

$$\begin{aligned} & \left( \hat{F}_m^{(+, tot)} \right)_{11} H_{y||m}^{(t)} - \left( \hat{F}_m^{(-, tot)} \right)_{11} H_y^{(i)} \delta_{m,0} \\ & - \left( \hat{F}_m^{(-, tot)} \right)_{12} H_{y||m}^{(r)} = -\frac{4\pi}{c} j_{x||m}, \end{aligned} \quad (16)$$

where

$$\begin{aligned} j_{x||m} &= \frac{2(2 - \delta_{m,0})}{D} \int_0^{W/2} j_x(x) \cos \left( \frac{2\pi m}{D} x \right) dx \\ &= j_x(0) \frac{2 - \delta_{m,0}}{2m} J_1 \left( \frac{m\pi W}{D} \right) \end{aligned} \quad (17)$$

is the Fourier component of current density, and  $J_1(\cdot)$  is the Bessel function. In the similar manner, using boundary conditions for electric field's tangential component, we obtain

$$\begin{aligned} & \left( \hat{F}_m^{(+, tot)} \right)_{21} H_{y||m}^{(t)} - \left( \hat{F}_m^{(-, tot)} \right)_{21} H_y^{(i)} \delta_{m,0} \\ & - \left( \hat{F}_m^{(-, tot)} \right)_{22} H_{y||m}^{(r)} = 0. \end{aligned} \quad (18)$$

From Eqs. (16) and (18) it is possible to express amplitudes for the transmitted and reflected harmonics as

$$H_{y||m}^{(r)} = -\frac{f_0}{g_0 \left( \hat{F}_0^{(-,tot)} \right)_{22} \left( \hat{F}_0^{(+,tot)} \right)_{21}} H_y^{(i)} \delta_{m,0} - \frac{1}{g_m \left( \hat{F}_m^{(-,tot)} \right)_{22}} \frac{4\pi}{c} j_{x||m}, \quad (19)$$

$$H_{y||m}^{(t)} = -\frac{2}{g_0 \left( \hat{F}_0^{(-,tot)} \right)_{22} \left( \hat{F}_0^{(+,tot)} \right)_{21}} H_y^{(i)} \delta_{m,0} - \frac{1}{g_m \left( \hat{F}_m^{(+,tot)} \right)_{21}} \frac{4\pi}{c} j_{x||m}, \quad (20)$$

where  $f_0 = \left( \hat{F}_0^{(+,tot)} \right)_{11} \left( \hat{F}_0^{(-,tot)} \right)_{21} - \left( \hat{F}_0^{(-,tot)} \right)_{11} \left( \hat{F}_0^{(+,tot)} \right)_{21}$  and  $g_m = \left( \hat{F}_m^{(+,tot)} \right)_{11} / \left( \hat{F}_m^{(+,tot)} \right)_{21} - \left( \hat{F}_m^{(-,tot)} \right)_{12} / \left( \hat{F}_m^{(-,tot)} \right)_{22}$ . On the other hand, current density in graphene strips can be expressed via the Ohm law as

$$j_x(x) = \sigma_g(\omega) \sum_{l=-\infty}^{\infty} \Theta\left(\frac{W}{2} - |x - lD|\right) E_x^{(4)}(x, 0),$$

where the graphene's conductivity  $\sigma_g(\omega)$  is supposed to be of Drude type,

$$\sigma_g(\omega) = \frac{e^2}{\hbar^2 \pi} \frac{E_F}{\gamma - i\omega}.$$

Here  $E_F$  is the Fermi energy,  $\gamma$  is the inverse relaxation rate,  $e$  is the electron charge, and  $\hbar$  is the Planck constant. In this case the average value of current on the period can be represented in the form

$$\begin{aligned} j_{x||0} &= \frac{2}{D} \int_0^{D/2} j_x(x) dx \\ &= \sigma_g(\omega) \sum_{m=0}^{\infty} \frac{\sin\left(\frac{m\pi W}{D}\right)}{m\pi} \left( \hat{F}_m^{(+,tot)} \right)_{21} H_{y||m}^{(t)}. \end{aligned}$$

Combining this expression with the explicit form of  $j_{x||m}$  [see Eq. (17)] and  $H_{y||m}^{(t)}$  [see Eq. (20)], it is possible to obtain an expression for current density at the center of the strip,

$$\begin{aligned} j_x(0) &= -\sigma_g(\omega) \frac{8}{g_0 \pi} \frac{H_y^{(i)}}{\left( \hat{F}_0^{(-,tot)} \right)_{22}} \left\{ 1 + \frac{8}{c} \sigma_g(\omega) \right. \\ &\times \left. \sum_{m=0}^{\infty} \frac{D \sin\left(\frac{m\pi W}{D}\right)}{W m \pi} \frac{1}{g_m} \frac{2 - \delta_{m,0}}{m} J_1\left(\frac{m\pi W}{D}\right) \right\}^{-1}. \end{aligned} \quad (21)$$

This equation, jointly with Eqs. (17), (19), and (20) allows calculation of the amplitudes of spatial harmonics of the transmitted and reflected wave  $H_{y||m}^{(t)}$ ,  $H_{y||m}^{(r)}$ . For the limiting case of continuous graphene,  $W = D$ , absence of analyte, and absence of both hBN layers [when total field matrices are  $\hat{F}_m^{(\pm, tot)} = \hat{F}_m$ ] the current density (21) will be represented in the simple form

$$j_x(0) = \frac{\sigma_g(\omega) \frac{4}{\pi} H_y^{(i)}}{1 + \frac{2\pi}{c} \sigma_g(\omega)}. \quad (22)$$

Respectively, the amplitudes of the reflected and transmitted waves (zeroth harmonics) are

$$\begin{aligned} H_{y||0}^{(r)} &= \frac{\frac{2\pi}{c} \sigma_g(\omega) H_y^{(i)}}{1 + \frac{2\pi}{c} \sigma_g(\omega)}, \\ H_{y||0}^{(t)} &= \frac{H_y^{(i)}}{1 + \frac{2\pi}{c} \sigma_g(\omega)}, \end{aligned}$$

which coincide with the previous results for the case of continuous graphene[70].

Further in the paper the electromagnetic properties of the structure will be characterized by the reflectance, transmittance, and absorbance, which are related to the energy flux, whose absolute value and direction are described by the Poynting vector  $\mathbf{S} = (c/8\pi) \text{Re} [\mathbf{E} \times \overline{\mathbf{H}}]$ , where overbar stands for complex conjugation, and  $\times$  stands for the vector product. Since incident wave propagates along  $z$ -axis, integral reflection (transmission) coefficient is proportional to  $z$ -component of the reflected (transmitted) wave's Poynting vector, averaged on half-period,

$$S_z^{(r,t)}(z) = (c/8\pi) \int_0^{D/2} dx E_x^{(r,t)}(x, z) \overline{H_y^{(r,t)}(x, z)}. \quad (23)$$

Electromagnetic fields of the reflected wave can be obtained from the second column of the  $2 \times 2$  matrix in Eq. (4), and after substituting them into Eq. (23), the respective component of Poynting vector has the form

$$S_z^{(r)} = \frac{cD}{16\pi} \text{Re} \left\{ \sum_{m=0}^{\infty} \left( \hat{F}_m \right)_{22} \frac{1 + \delta_{m,0}}{2} \left| H_{y||m}^{(r)} \right|^2 \right\}. \quad (24)$$

In a similar manner for the transmitted wave [whose electromagnetic field can be obtained from the first column of the  $2 \times 2$  matrix in Eq. (5)], we have

$$S_z^{(t)} = \frac{cD}{16\pi} \text{Re} \left\{ \sum_{m=0}^{\infty} \left( \hat{F}_m \right)_{21} \frac{1 + \delta_{m,0}}{2} \left| H_{y||m}^{(t)} \right|^2 \right\}. \quad (25)$$

Notice, that  $S_z^{(r,t)}$  in vacuum are independent of distances owing to the absence of losses. Taking into account the Poynting vector's  $z$ -component of incident wave  $S_z^{(i)} = cD \left| H_y^{(i)} \right|^2 / (16\pi)$  [whose electromagnetic field can be taken from the first column of the  $2 \times 2$  matrix in Eq. (4)], we define the integral reflectance  $R$  and transmittance  $T$  of the structure as relations

$$R = -\frac{S_z^{(r)}}{S_z^{(i)}} = -\frac{\text{Re} \left\{ \sum_{m=0}^{\infty} \left( \hat{F}_m \right)_{22} \frac{1 + \delta_{m,0}}{2} \left| H_{y||m}^{(r)} \right|^2 \right\}}{\left| H_y^{(i)} \right|^2}, \quad (26)$$

$$T = \frac{S_z^{(t)}}{S_z^{(i)}} = \frac{\text{Re} \left\{ \sum_{m=0}^{\infty} \left( \hat{F}_m \right)_{21} \frac{1 + \delta_{m,0}}{2} \left| H_{y||m}^{(t)} \right|^2 \right\}}{\left| H_y^{(i)} \right|^2}. \quad (27)$$

The minus sign in Eq. (26) accounts for the negative direction of the reflected wave propagation.

### 3 Eigenmodes of surface phonon-plasmon-polaritons

The dispersion relation for eigenmodes of the equivalent structure with continuous graphene, shown in Fig. 1(b) can formally be obtained from Eqs. (16) and (18) by formal substitution  $2\pi m/D = k_x$  and Ohm's law for continuous graphene  $j_{x||m} = \sigma_g(\omega) \left( \hat{F}_m^{(+,tot)} \right)_{21} H_{y||m}^{(t)}$ . For the case without external wave  $H_y^{(i)} \equiv 0$  (condition for the eigenmodes), the dispersion relations will have the form

$$1 + \frac{4\pi}{cg_m} \sigma_g(\omega) = 0. \quad (28)$$

The spectrum of the equivalent structure [Fig. (1)(b)] can be obtained as solution of the dispersion relation (28), and in the vicinity of the upper RB consists of infinite number of modes [first five of which are shown in Figs. 2(a), 2(b)], which start at the lower<sup>2</sup> edge of RB  $\lambda \approx 7.3 \mu\text{m}$  (where  $\varepsilon_{xx} = 0$ ). In the case of the undoped graphene all the spectrum [dashed lines] except the first mode [red dashed line] lies in the frequency domain  $6.22 \mu\text{m} \lesssim \lambda \lesssim 7.3 \mu\text{m}$ , where  $\varepsilon_{xx} < 0$ , and asymptotically approaches the RB upper edge [see inset in Fig. 2(a)]. The first mode with lowest  $k_x$  [red

<sup>2</sup>Lower and upper edges are characterized in terms of frequency, hence, the free-space wavelength of upper edge is shorter than that of lower edge.

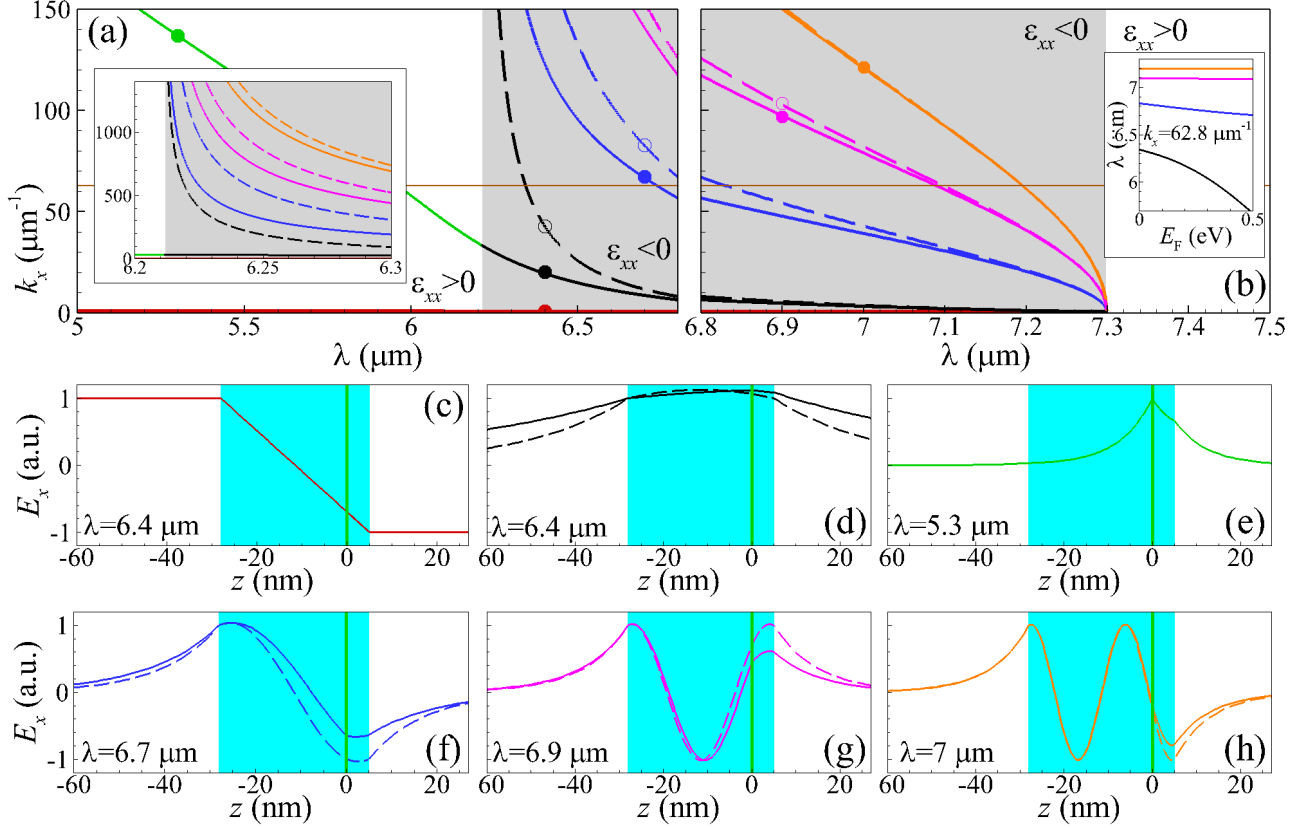


Figure 2: (a)-(b) Spectrum of the phonon-plasmon polaritons (five lower modes) in the structure with continuous graphene [shown in Fig. 1(b)] in the vicinity of hBN upper restrahlen band for undoped graphene (dashed lines) and doped graphene (solid lines). Horizontal brown solid line correspond to the wavevector  $k_x = 62.8 \mu\text{m}^{-1}$ . In panel (a) inset shows zoom of dispersion curves near asymptotics, while inset in panel (b) demonstrates the dependence of eigenmode free-space wavelength upon Fermi energy for fixed value of in-plane wavevector  $k_x$ ; (c)-(h) Spatial profiles of the electric field's  $x$ -component  $E_x$  of first [panel (c)], second [panels (d) and (e)], third [panel (f)], fourth [panel (g)] and fifth [panel (h)] eigenmodes for undoped (dashed lines) and doped (solid lines) graphene. Parameters (free-space wavelength  $\lambda$  and in-plane wavevector  $k_x$ ) of eigenmodes, depicted in panels (c)–(h) are shown in panel (a) and (b) by filled (empty) circles for doped (undoped) graphene. Areas, occupied by h-BN are shaded in panels (c)–(h) by blue color, while position of graphene is depicted by green vertical line. In all panels other parameters are:  $d_t = 28 \text{ nm}$ ,  $d_b = 5 \text{ nm}$ , and the Fermi energy of doped graphene  $E_F = 0.35 \text{ eV}$ .

line in Figs.2(a) and 2(b)] lies nearby the light line in vacuum  $k_x = \omega/c$ . As a result, it is characterized by weak decay of its electric field inside the vacuum and is antisymmetric inside hBN-graphene slab [see spatial profile in Fig. 2(c)]. Other modes differ from each other by the number of variations of sign of electric field across the hBN layer [as shown in Figs. 2(c)–2(h)], which is typical for dielectric waveguide modes (further in the paper such kind of modes will be referred as waveguide-like). Thus, the second mode [black dashed lines in Figs. 2(a)–2(b)] is characterized by absence of sign variation, while third (blue line), fourth (pink line) and fifth (orange line) modes exhibit one, two, and three sign variation, respectively [see Figs. 2(d), 2(f), 2(g), and 2(h)]. Doping of graphene results in the lowering of free-space wavelengths  $\lambda$  of all modes [see inset in Fig. 2(b)]. At the same time, only third and higher modes [solid blue, pink, and orange lines in Figs. 2(a)–2(b)] asymptotically approaches the upper edge of RB, while the second mode (solid black line) at RB's upper edge transforms into the plasmon-like mode (green line), which exists beyond the RB and is absent in the case of undoped graphene. The plasmon-like nature of this mode is defined by the fact that its electromagnetic field [see Fig. 2(e)] is localized nearby the graphene layer, while waveguide-like modes are localized inside the hBN slab [solid lines in Figs. 2(d), 2(f), 2(g), and 2(h)]. Notice, that graphene's doping slightly perturbs the electromagnetic field spatial distributions [compare dashed and solid lines in Figs. 2(d), 2(f), 2(g), and 2(h)], while numbers of sign variations are kept unchanged.

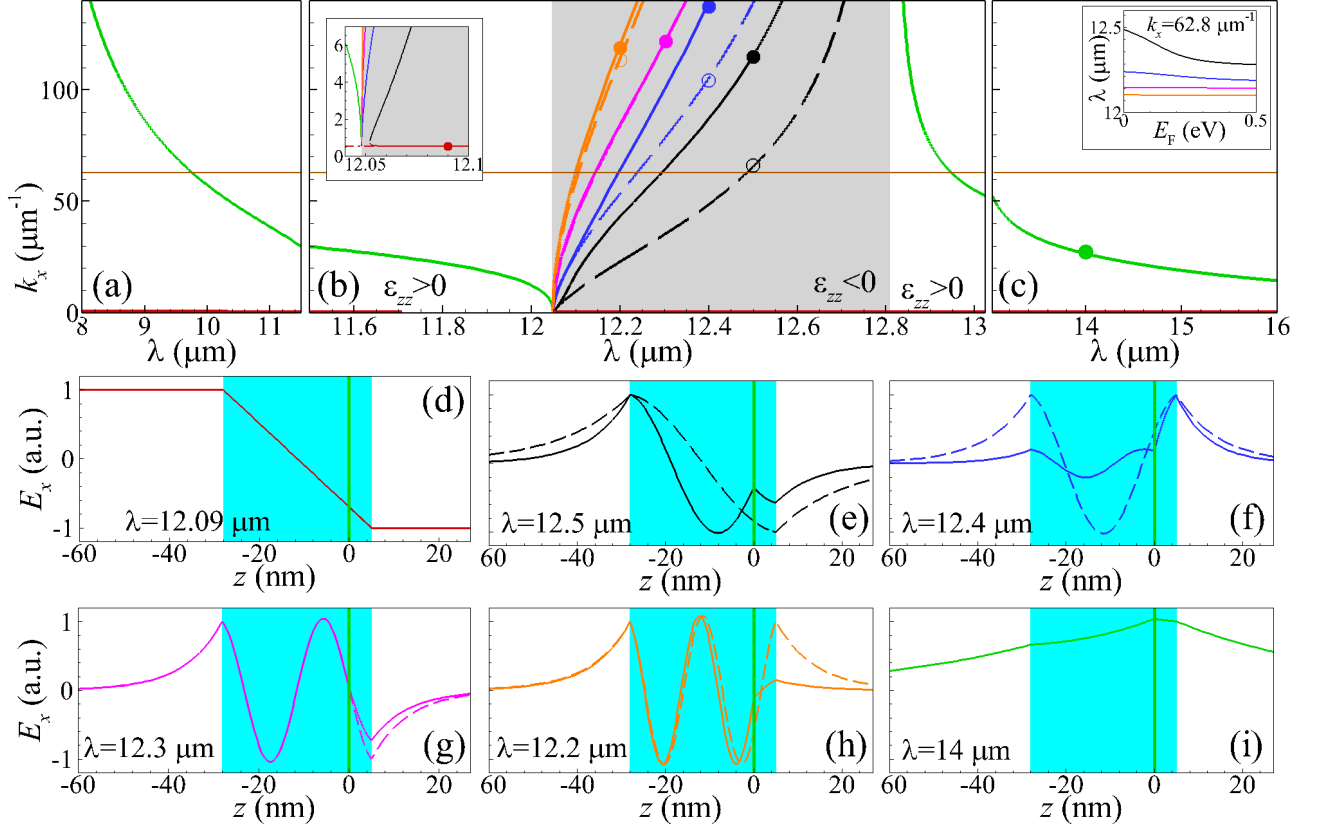


Figure 3: (a)–(c) Spectrum of the phonon-plasmon polaritons (five lower modes) in the structure with continuous graphene [shown in Fig. 1(b)] in the vicinity of hBN lower reststrahlen band for undoped graphene (dashed lines) and doped (solid lines) graphene (solid lines). In panel (b) inset shows zoom of dispersion curves near the bifurcation point between first and second modes, while inset in panel (c) demonstrates the dependence of eigenmode free-space wavelength upon Fermi energy for fixed value of in-plane wavevector  $k_x$ ; (c)–(h) Spatial profiles of the electric field's  $x$ -component  $E_x$  of first [panel (d)], second [panel (e)], third [panel (f)], fourth [panel (g)], and fifth [panel (h)] eigenmodes and as well as eigenmode inside the gap [panel (i)] for undoped (dashed lines) and doped (solid lines) graphene. Parameters (free-space wavelength  $\lambda$  and in-plane wavevector  $k_x$ ) of eigenmodes, depicted in panels (d)–(i) are shown in panel (a) and (b) by filled (empty) circles for doped (undoped) graphene. Other parameters as well as meaning of horizontal lines in panels (a)–(c) and of shaded areas and vertical lines in panels (d)–(i) are the same as those in Fig. 2.

Another plasmonic-like mode exist in the gap between upper and lower RBs [green line in Figs. 3(a) and 3(b)], which starts at the upper edge of the lower RB. At the same time, third and higher waveguide modes [blue, pink, and orange lines in Fig. 3(b)] also have origin at the upper edge of the lower RB, while the first and second waveguide modes (depicted by red and black lines, respectively) have common bifurcation point [see inset in Fig. 3(b)]. All the waveguide modes (except first one) approach asymptotically lower edge of the lower RB, while first one exists inside the lower gap both in the case of doped and undoped graphene. At the same time, for the case of doped graphene lower gap contains also a plasmon-like mode [depicted by green solid line in Figs. 3(b) and 3(c), and which field is shown in Fig. 3(i)]. Similar to the case of upper RB graphene doping lowers the free-space wavelengths  $\lambda$  of all modes [see inset in Fig. 3(c)], and perturbs the field spatial distribution [Figs. 3(d)–3(h)]. Along with this, unlike the previous case (upper RB), in the case of lower RB there is no mode with absence of sign variation.

#### 4 Absorbance spectrum of graphene nanoribbon periodic array

All the eigenmodes (both waveguide and plasmonic), depicted in Figs. 2(c)–2(h) and 3(d)–3(i) are evanescent waves inside the spatial domains occupied by vacuum. This fact means the impossibility to couple these modes directly to an external propagating wave. However, they can be coupled to the diffracted harmonics of a periodic grating. In this

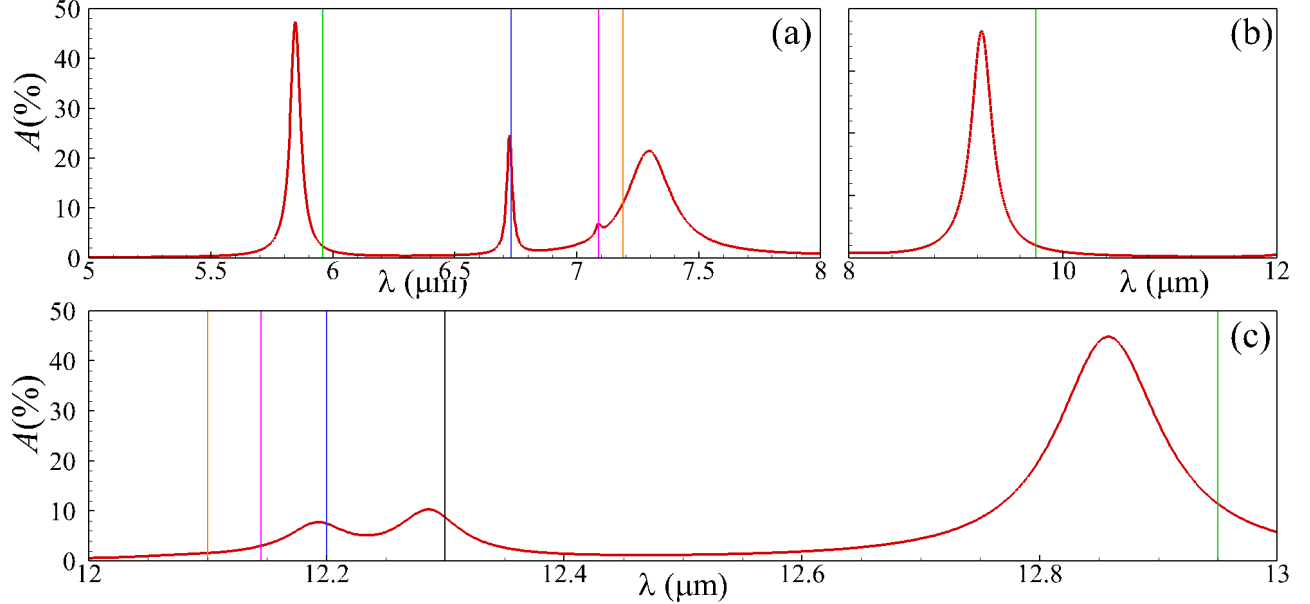


Figure 4: Dependence of plane-wave absorbance  $A$  upon free-space wavelength  $\lambda$  of the periodical structure without analyte layer [depicted in Fig. 1(a)]. The parameters of the structure are:  $D = 100$  nm,  $W = 50$  nm,  $E_F = 0.7$  eV,  $d_a = 0$ ,  $d_t = 28$  nm,  $d_b = 5$  nm. Vertical lines depict free-space wavelengths of eigenmodes of equivalent structure [depicted in Fig. 1(b)] for fixed wavevector  $k_x = 2\pi/D$ , namely second (black lines), third (blue lines), fourth (pink lines), and fifth (orange lines) inside the restrahlen bands and eigenmode outside restrahlen bands (green lines).

case the in-plane component of the incident wave will be effectively elongated by an integer number of the reciprocal grating vectors. For example, if  $D$  is the period of the grating, then normally incident external wave can excite those modes in the spectrum, which wavevectors are equal to  $k_x = 2\pi m/D$  (here  $m$  is an integer number). For the particular value of the period  $D = 100$  nm the free-space wavelengths, at which mode excitation is possible, can be estimated as crossing points between the spectrum [shown in Figs. 2(a), 2(b), 3(a)–3(c)] and horizontal solid brown lines (which correspond to the wavevector  $k_x = 2\pi/D$  of first harmonic with  $m = 1$ ). The values of these predicted free-space wavelengths are depicted by vertical lines in Fig. 4, while the calculated absorbance is shown by the solid red line. This absorbance spectrum is calculated for the Fermi energy of graphene strips  $E_F = 0.7$  eV in order to have average Fermi energy on period  $E_F(W/D)$  equal to that, used in Figs. 2 and 3. As it is seen, the absorbance spectrum contains various peaks, which correspond to different eigenmodes excitation (for comparison, in the case of graphene without hBN the absorbance spectrum would contain only one peak, see Ref.[51]). It is interesting, that positions of peaks coincide well with the eigenmode frequencies for the case of waveguide-like modes [blue and pink solid lines in Fig. 4(a) as well blue and black lines in Fig. 4(c)], but slightly differs from the predicted ones in the case of plasmonic-like modes. The reason for such a behaviour is that waveguide-like modes are localized inside the whole hBN slab, thus influence of graphene patterning on mode properties being relatively small. At the same time, the plasmon-like modes are localized in the vicinity of graphene, where graphene patterning produces strong influence on the mode properties. An analysis of field distributions and their correspondence to eigenmode excitation is described in Supplemental document.

The position of absorption peaks, which correspond both to the excitation of waveguide-like and plasmon-like modes depend strongly upon the position of graphene inside the hBN slab, as it can be seen from Fig. 5. Thus, when graphene is relocated from the edge of the slab into its center, the position of the absorbance peaks are red-shifted.

In order to clarify the possibility of using this structure for sensing, we demonstrate in Fig. 6, that adding of the analyte layer on top of structure shifts positions of absorbance peaks. For the particular choice of parameters in Fig. 6, highest sensitivity to the variation of analyte layer thickness is observed for absorbance peaks nearby  $\lambda \sim 6.2$   $\mu\text{m}$ ,  $\lambda \sim 9.6$   $\mu\text{m}$ ,  $\lambda \sim 12.35$   $\mu\text{m}$ , and  $\lambda \sim 12.9$   $\mu\text{m}$ . These peaks correspond to the excitation of plasmon-like mode for wavelength below upper RB [green line in Fig. 2(a)], plasmon-like mode between RBs [green lines in Figs. 3(a) and 3(b)], second waveguide-like mode in lower RB [black line in Fig. 3(b)] and plasmon-like mode below lower RB [green line in Figs. 3(b) and 3(c)], respectively. For these peaks the significant shift takes place already at the analyte thicknesses  $d_a \sim 20$  nm, while further increase of analyte thickness does not influence position of these peaks, owing to the rapid decay of field intensity away from interface between top hBN layer and analyte. At the same time the absorbance peaks nearby  $\lambda \sim 6.8$   $\mu\text{m}$ , which corresponds to the excitation of waveguide-like mode in upper RB [blue line in Figs. 2(a)

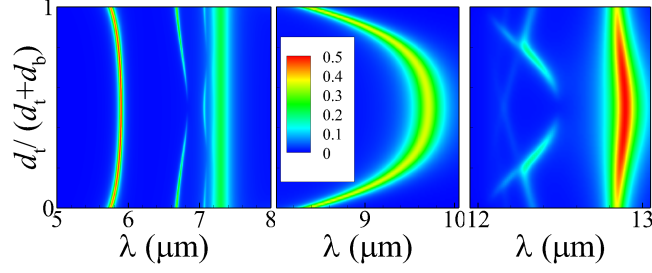


Figure 5: Plane-wave absorbance  $A$  versus free-space wavelength  $\lambda$  and relation between the thicknesses of top and bottom hBN layers  $d_t / (d_b + d_t)$  for the structure without analyte layer  $d_{\text{anal}} = 0$ . The total thickness of structure is kept fixed  $d_t + d_b = 33$  nm. Other parameters are the same as those in Fig. 4.

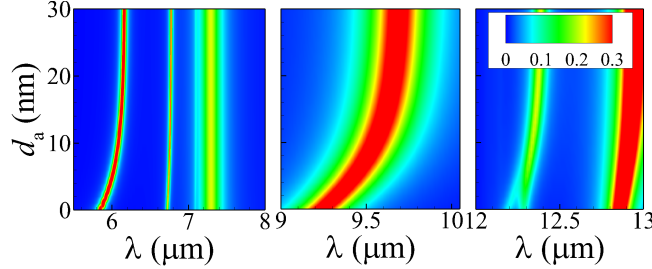


Figure 6: Absorbance (depicted by color map) versus free-space wavelength  $\lambda$  and thickness of analyte layer  $d_a$  for the case, where analyte refractive index  $n_a = 2$ . Other parameters are the same, as those in Fig. 4.

and 2(b)] is much less sensitive to the presence of analyte layer, while the peak nearby  $\lambda \sim 7.3 \mu\text{m}$  (mode bunching nearby edge of RB) is almost insensitive. Notice, with an increase of analyte layer thickness two waveguide-like modes [corresponding to the black and blue lines in Fig.3(b)] approximate to each other. The presence of highly analyte-sensitive and virtually analyte-insensitive absorption bands at the same spectral range can be beneficial for chemical/biosensing applications, as the insensitive bands can serve as a reference, as well as allow for reducing cross-sensitivity with, e.g., temperature variations.

In order to optimise the structure, in Fig. 7 we depict the dependence of absorbance upon the relative position of graphene inside the hBN layer. From this figure it is clear, that maximal shift of the plasmon-like mode below RBs (nearby  $\lambda \sim 13 \mu\text{m}$ ) takes place, when graphene is arranged in the center of the structure ( $d_t \approx d_b$ ). At the same time, for plasmon-like modes above RBs (nearby  $\lambda \sim 6 \mu\text{m}$ ) and between RBs (nearby  $8 \mu\text{m} \lesssim \lambda \lesssim 10 \mu\text{m}$ ) relative shifts of absorbance peaks (if compared to one without analyte layer, which absorbance maxima are shown by white lines) are maximal, when graphene is close to the analyte layer. Thus, when top hBN layer is absent,  $d_t = 0$ , the maximal shift of resonance at  $n_a = 1$  and  $n_a = 2$  is  $\Delta\lambda \approx 9.37 \mu\text{m} - 8.37 \mu\text{m} = 1 \mu\text{m}$ , or  $\Delta\omega \approx 130 \text{cm}^{-1}$ , which is compatible to experimentally observed in Ref.[62]. In more details this phenomenon is shown in middle column of Fig. 8, where for  $d_t = 30$  nm [Fig. 8(b1)] the shift of resonance at  $n_a = 1$  and  $n_a = 2$  is indistinguishable in the scale of panel, while for  $d_t = 3$  nm and the same analyte layer thickness [Figs. 8(b2)] the sensitivity[71]  $S = \Delta\lambda / \Delta n_a \approx 560$  nm/RIU with figure-of-merit  $\text{FoM} = S / \Delta\lambda_{0.5} \approx 2.6$  RIU $^{-1}$ , with  $\Delta\lambda_{0.5}$  being the width of the resonance at half-maximum[72]. This value of sensitivity exceeds the theoretical estimation, given in Ref.[54], while FoM is compatible with Ref.[54]. For the thinner analyte layer  $d_a = 5$  nm [Fig. 8(b3)] the sensitivity is diminished considerably  $S \approx 250$  nm/RIU. The same situation takes place for plasmon-like mode above RB: when graphene is arranged nearby the hBN layer's edge, opposite to analyte layer [Fig. 8(a1)], the sensitivity of this mode is  $S \approx 30$  nm/RIU. Nevertheless, when graphene is close to the analyte layer [Fig. 8(a2)] the sensitivity becomes considerably larger  $S \approx 370$  nm/RIU [with  $\text{FoM} \approx 7.75$  RIU $^{-1}$  which is considerably higher if compared to that in Fig. 8(b2) owing to narrower resonance] for the same analyte layer thickness and  $S \approx 200$  nm/RIU for thinner analyte layer [see Fig. 8(a3)]. At the same time, the sensitivity of third waveguide-like mode in lower RB, located nearby  $\lambda \sim 6.7 \mu\text{m}$ , is almost equal  $S \approx 60$  nm/RIU both for the case  $d_t = 30$  nm,  $d_b = 3$  nm [Fig. 8(a1)] and for the case  $d_t = 3$  nm,  $d_b = 30$  nm [Fig. 8(a2)], owing to the field distribution inside all hBN slab. In the upper RB an interesting phenomenon takes place: when graphene layer is located nearby analyte [Figs. 8(c2) and 8(c3)] the second waveguide-like mode, located nearby  $\lambda \sim 12.3 \mu\text{m}$  is almost insensitive to the presence of analyte layer, while third waveguide-like mode (nearby  $\lambda \sim 12.1 \mu\text{m}$ ) exhibits the sensitivities  $S \approx 110$  nm/RIU and  $S \approx 40$  nm/RIU for  $d_a = 20$  nm and  $d_a = 5$  nm, respectively. At the same time,

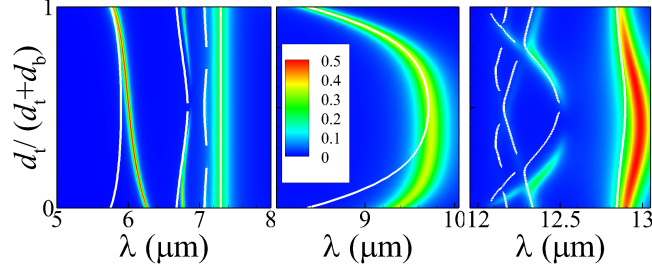


Figure 7: Plane-wave absorbance  $A$  versus free-space wavelength  $\lambda$  and relation between the thicknesses of top and bottom hBN layers  $d_t / (d_b + d_t)$  for the structure with analyte layer of thickness  $d_a = 20$  nm and refractive index  $n_a = 2$ . The total thickness of structure is kept fixed  $d_t + d_b = 33$  nm. Other parameters are the same as those in Fig. 4. The position of absorbance peak maxima of structure without analyte layer are depicted by white solid lines.

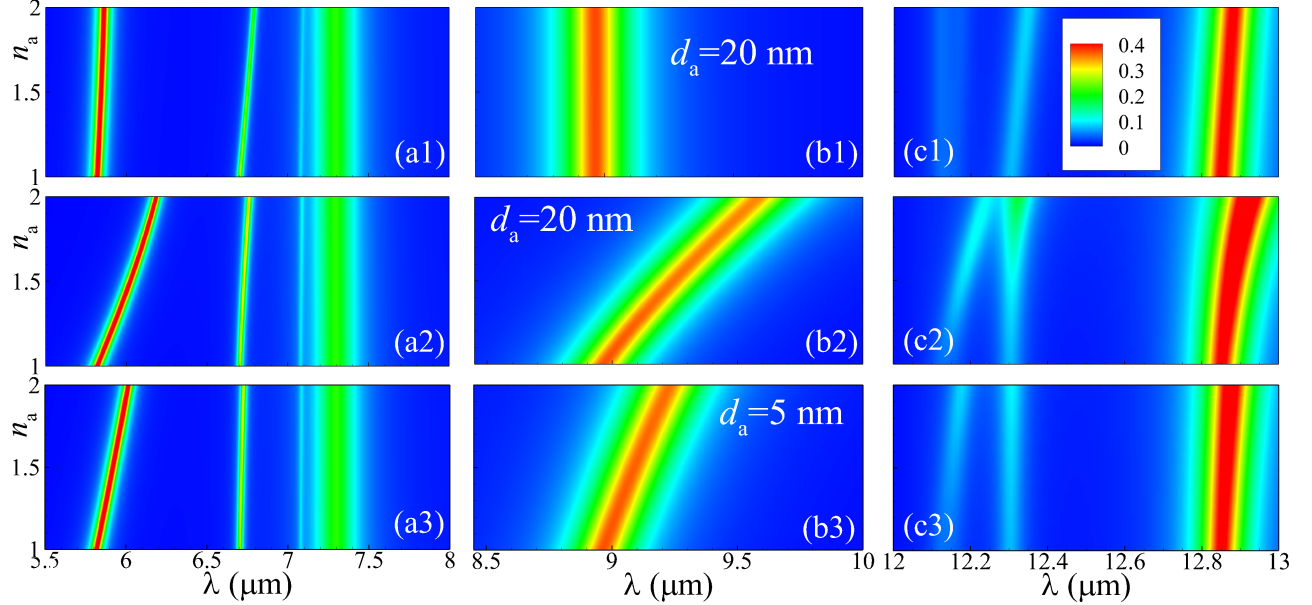


Figure 8: Absorbance (depicted by color map) versus free-space wavelength  $\lambda$  and analyte refractive index  $n_a$  for two values of analyte layer thickness  $d_a = 20$  nm [top and middle rows, panels (a1)–(c1), (a2)–(c2)], and  $d_a = 5$  nm [bottom row, panels (a3)–(c3)] and hBN layers thicknesses  $d_t = 30$  nm,  $d_b = 3$  nm [top row, panels (a1)–(c1)] and  $d_t = 3$  nm,  $d_b = 30$  nm [middle and bottom rows, panels (a2)–(c2), (a3)–(c3)]. Other parameters are the same, as those in Fig. 4.

when graphene layer is arranged at the edge of hBN slab, opposite to analyte layer [Figs. 8(c1)] the situation is opposite: here second-waveguide-like mode is almost insensitive to the presence of analyte layer, while third one exhibits the sensitivity  $S \approx 50$  nm/RIU.

## 5 Conclusions

In the present paper we investigated theoretically the coupling of an external plane electromagnetic wave to diffraction grating, consisting of a periodic array of graphene nanoribbons, clad by two layers of hBN. We demonstrate, that the absorbance spectrum of this structure exhibits a series of peaks, related to the excitation of eigenmodes. We also showed, that this structure can be potentially used in the sensing applications. In detail, deposition of an analyte dielectric layer of relatively small thickness  $\sim 20$  nm on top of this structure results in the considerable shift of several absorbance peak positions. The peak, related to the excitation of the plasmon-like eigenmode between RBs, demonstrates the maximal shift  $\sim 1000$  nm/RIU in the case, when graphene nanoribbon array is located in the vicinity of analyte layer. Further increase of sensitivity can be achieved by the patterning of graphene in more complicated manner, like flower-shape[73], split-ring resonators [74], crosses [75, 76] among others. Another potential application of these graphene-hBN hybrid

structures is to be building blocks of a new class of photodetectors [77, 78], where these structures serve simultaneously as active media, sustaining phonon-plasmon polaritons and as key-element of the detector.

## Acknowledgments

C. J. S. dM. and D. A. B. acknowledge financial support by FAPESP (grant no. 2018/07276-5), FINEP (grant no. 01.22.0208.00), the Brazilian Nanocarbon Institute of Science and Technology (INCT/Nanocarbon), and CAPES-PrInt (grant nos. 88887.310281/2018-00 and 88881.310294/2018-01). Y. V. B. and N. M. R. P. acknowledge support by the Portuguese Foundation for Science and Technology (FCT) in the framework of the Strategic Funding UIDB/04650/2020, COMPETE 2020, PORTUGAL 2020, FEDER. N. M. R. P. also acknowledges support by FCT through projects PTDC/FIS-MAC/2045/2021 (10.54499/PTDC/FIS-MAC/2045/2021) and EXPL/FIS-MAC/0953/2021, as well as the Independent Research Fund Denmark (grant no. 2032-00045B) and the Danish National Research Foundation (Project No. DNRF165).

## Disclosures

The authors declare no conflicts of interest.

## References

- [1] D N Basov, Ana Asenjo-Garcia, P James Schuck, Xiaoyang Zhu, and Angel Rubio. Polariton panorama. *Nanophotonics*, 10(1):549–577, nov 2020. ISSN 2192-8614. doi:10.1515/nanoph-2020-0449. URL <https://www.degruyter.com/document/doi/10.1515/nanoph-2020-0449/html>.
- [2] J M Pitarke, V M Silkin, E V Chulkov, and P M Echenique. Theory of surface plasmons and surface-plasmon polaritons. *Reports on Progress in Physics*, 70(1):1–87, jan 2007. ISSN 0034-4885. doi:10.1088/0034-4885/70/1/R01. URL <http://stacks.iop.org/0034-4885/70/i=1/a=R01>.
- [3] Junxi Zhang, Lide Zhang, and Wei Xu. Surface plasmon polaritons: physics and applications. *Journal of Physics D: Applied Physics*, 45(11):113001, mar 2012. ISSN 0022-3727. doi:10.1088/0022-3727/45/11/113001. URL <https://iopscience.iop.org/article/10.1088/0022-3727/45/11/113001>.
- [4] Rana Sadaf Anwar, Huansheng Ning, and Lingfeng Mao. Recent advancements in surface plasmon polaritons-plasmonics in subwavelength structures in microwave and terahertz regimes. *Digital Communications and Networks*, 4(4):244–257, 2018. ISSN 23528648. doi:10.1016/j.dcan.2017.08.004. URL <https://doi.org/10.1016/j.dcan.2017.08.004>.
- [5] Joshua D Caldwell, Lucas Lindsay, Vincenzo Giannini, Igor Vurgaftman, Thomas L Reinecke, Stefan A Maier, and Orest J Glembocki. Low-loss, infrared and terahertz nanophotonics using surface phonon polaritons. *Nanophotonics*, 4(1):44–68, apr 2015. ISSN 2192-8614. doi:10.1515/nanoph-2014-0003. URL <https://www.degruyter.com/document/doi/10.1515/nanoph-2014-0003/html>.
- [6] Alexey Kavokin. Exciton-polaritons in microcavities: Recent discoveries and perspectives. *physica status solidi (b)*, 247(8):1898–1906, aug 2010. ISSN 03701972. doi:10.1002/pssb.200983955. URL <https://onlinelibrary.wiley.com/doi/10.1002/pssb.200983955>.
- [7] D L Mills and E Burstein. Polaritons: the electromagnetic modes of media. *Reports on Progress in Physics*, 37(7):817–926, jul 1974. ISSN 0034-4885. doi:10.1088/0034-4885/37/7/001. URL <http://stacks.iop.org/0034-4885/37/i=7/a=001?key=crossref.283477515fe65a3451f4b9836b4d0f65>.
- [8] R.E. Camley. Nonreciprocal surface waves. *Surface Science Reports*, 7(3-4):103–187, jul 1987. ISSN 01675729. doi:10.1016/0167-5729(87)90006-9. URL <http://linkinghub.elsevier.com/retrieve/pii/0167572987900069>.
- [9] Frank H.L. Koppens, Darrick E Chang, and F. Javier García de Abajo. Graphene Plasmonics: A Platform for Strong Light-Matter Interactions. *Nano Letters*, 11(8):3370–3377, aug 2011. ISSN 1530-6984. doi:10.1021/nl201771h. URL <http://arxiv.org/abs/1104.2068><http://pubs.acs.org/doi/abs/10.1021/nl201771h>.
- [10] Sanshui Xiao, Xiaolong Zhu, Bo-Hong Li, and N. Asger Mortensen. Graphene-plasmon polaritons: From fundamental properties to potential applications. *Frontiers of Physics*, 11(2):117801, apr 2016. ISSN 2095-0462. doi:10.1007/s11467-016-0551-z. URL <http://link.springer.com/10.1007/s11467-016-0551-z>.
- [11] Alexey Yu. Nikitin, F Guinea, Francisco J. García-Vidal, and Luis Martín-Moreno. Fields radiated by a nanoemitter in a graphene sheet. *Physical Review B*, 84(19):195446, nov 2011. ISSN 1098-0121.

- doi:10.1103/PhysRevB.84.195446. URL <http://arxiv.org/abs/1104.3558><http://link.aps.org/doi/10.1103/PhysRevB.84.195446>.
- [12] Siyuan Dai, Wenjing Fang, Nicholas Rivera, Yijing Stehle, Bor-Yuan Jiang, Jialiang Shen, Roland Yingjie Tay, Christopher J. Ciccario, Qiong Ma, Daniel Rodan-Legrain, Pablo Jarillo-Herrero, Edwin Hang Tong Teo, Michael M. Fogler, Prineha Narang, Jing Kong, and Dimitri N. Basov. Phonon Polaritons in Monolayers of Hexagonal Boron Nitride. *Advanced Materials*, 31(37):1806603, sep 2019. ISSN 0935-9648. doi:10.1002/adma.201806603. URL <https://onlinelibrary.wiley.com/doi/10.1002/adma.201806603>.
- [13] Fengrui Hu and Zhe Fei. Recent Progress on Exciton Polaritons in Layered Transition-Metal Dichalcogenides. *Advanced Optical Materials*, 8(5):1901003, mar 2020. ISSN 2195-1071. doi:10.1002/adom.201901003. URL <https://onlinelibrary.wiley.com/doi/10.1002/adom.201901003>.
- [14] Tony Low and Phaedon Avouris. Graphene Plasmonics for Terahertz to Mid-Infrared Applications. *ACS Nano*, 8(2):1086–1101, feb 2014. ISSN 1936-0851. doi:10.1021/nn406627u. URL <http://pubs.acs.org/doi/abs/10.1021/nn406627u>.
- [15] Marta Klanjšek Gunde. Vibrational modes in amorphous silicon dioxide. *Physica B: Condensed Matter*, 292(3-4):286–295, nov 2000. ISSN 09214526. doi:10.1016/S0921-4526(00)00475-0. URL <https://linkinghub.elsevier.com/retrieve/pii/S0921452600004750>.
- [16] L. M. Zhang, G. O. Andreev, Z. Fei, A. S. McLeod, G. Dominguez, M. Thiemens, A. H. Castro-Neto, D. N. Basov, and M. M. Fogler. Near-field spectroscopy of silicon dioxide thin films. *Physical Review B*, 85(7):075419, feb 2012. doi:10.1103/physrevb.85.075419.
- [17] T. Q.P. Vuong, S. Liu, A. Van Der Lee, R. Cuscó, L. Artús, T. Michel, P. Valvin, J. H. Edgar, G. Cassabois, and B. Gil. Isotope engineering of van derWaals interactions in hexagonal boron nitride. *Nature Materials*, 17(2):152–158, 2018. ISSN 14764660. doi:10.1038/NMAT5048.
- [18] Yongqing Cai, Litong Zhang, Qingfeng Zeng, Laifei Cheng, and Yongdong Xu. Infrared reflectance spectrum of BN calculated from first principles. *Solid State Communications*, 141(5):262–266, feb 2007. ISSN 00381098. doi:10.1016/j.ssc.2006.10.040. URL <https://linkinghub.elsevier.com/retrieve/pii/S0038109806009719>.
- [19] Mingze He, Lucas Lindsay, Thomas E. Beechem, Thomas Folland, Joseph Matson, Kenji Watanabe, Andrey Zavalin, Akira Ueda, Warren. E. Collins, Takashi Taniguchi, and Joshua D. Caldwell. Phonon engineering of boron nitride via isotopic enrichment. *Journal of Materials Research*, 36(21):4394–4403, nov 2021. ISSN 0884-2914. doi:10.1557/s43578-021-00426-9. URL <https://link.springer.com/10.1557/s43578-021-00426-9>.
- [20] R. J. Koch, T. Haensel, S. I.-U. Ahmed, Th. Seyller, and J. A. Schaefer. HREELS study of graphene formed on hexagonal silicon carbide. *physica status solidi c*, 7(2):394–397, feb 2010. ISSN 1862-6351. doi:10.1002/pssc.200982481. URL <https://onlinelibrary.wiley.com/doi/10.1002/pssc.200982481>.
- [21] Isaac John Luxmoore, Choon How Gan, Peter Qiang Liu, Federico Valmorra, Penglei Li, Jérôme Faist, and Geoffrey R. Nash. Strong Coupling in the Far-Infrared between Graphene Plasmons and the Surface Optical Phonons of Silicon Dioxide. *ACS Photonics*, 1(11):1151–1155, nov 2014. ISSN 2330-4022. doi:10.1021/ph500233s. URL <http://arxiv.org/abs/1405.7607><http://pubs.acs.org/doi/abs/10.1021/ph500233s>.
- [22] Thomas J. Constant, Samuel M. Hornett, Darrick E. Chang, and Euan Hendry. All-optical generation of surface plasmons in graphene. *Nature Physics*, 12(2):124–127, feb 2016. ISSN 1745-2473. doi:10.1038/nphys3545. URL <http://arxiv.org/abs/1505.00127><http://www.nature.com/doi/10.1038/nphys3545><http://www.nature.com/articles/nphys3545>.
- [23] R. J. Koch, Th. Seyller, and J. A. Schaefer. Strong phonon-plasmon coupled modes in the graphene/silicon carbide heterosystem. *Physical Review B*, 82(20):201413, nov 2010. ISSN 1098-0121. doi:10.1103/PhysRevB.82.201413. URL <https://link.aps.org/doi/10.1103/PhysRevB.82.201413>.
- [24] Zhe Fei, Gregory O Andreev, Wenzhong Bao, Lingfeng M Zhang, Alexander S McLeod, Chen Wang, Margaret K Stewart, Zeng Zhao, Gerardo Dominguez, Mark Thiemens, Michael M Fogler, Michael J Tauber, Antonio H Castro-Neto, Chun Ning Lau, Fritz Keilmann, and Dimitri N. Basov. Infrared Nanoscopy of Dirac Plasmons at the Graphene-SiO<sub>2</sub> Interface. *Nano letters*, pages 4701–4705, oct 2011. ISSN 1530-6992. doi:10.1021/nl202362d. URL <http://www.ncbi.nlm.nih.gov/pubmed/21972938>.
- [25] Yu Liu and R. F. Willis. Plasmon-phonon strongly coupled mode in epitaxial graphene. *Physical Review B*, 81(8):081406, feb 2010. ISSN 1098-0121. doi:10.1103/PhysRevB.81.081406. URL <https://link.aps.org/doi/10.1103/PhysRevB.81.081406>.

- [26] Victor W. Brar, Min Seok Jang, Michelle Sherrott, Seyoon Kim, Josue J. Lopez, Laura B. Kim, Mansoo Choi, and Harry Atwater. Hybrid Surface-Phonon-Plasmon Polariton Modes in Graphene/Monolayer h-BN Heterostructures. *Nano Letters*, 14(7):3876–3880, jul 2014. ISSN 1530-6984. doi:10.1021/nl501096s. URL <http://pubs.acs.org/doi/10.1021/nl501096s>.
- [27] Tony Low, Andrey Chaves, Joshua D. Caldwell, Anshuman Kumar, Nicholas X. Fang, Phaeton Avouris, Tony F. Heinz, Francisco Guinea, Luis Martín-Moreno, and Frank Koppens. Polaritons in layered two-dimensional materials. *Nature Materials*, 16(2):182–194, feb 2017. ISSN 1476-1122. doi:10.1038/nmat4792. URL <http://www.nature.com/articles/nmat4792>.
- [28] S. Dai, Q. Ma, T. Andersen, A. S. Mcleod, Z. Fei, M. K. Liu, M. Wagner, K. Watanabe, T. Taniguchi, M. Thiemens, F. Keilmann, P. Jarillo-Herrero, M. M. Fogler, and D. N. Basov. Subdiffractive focusing and guiding of polaritonic rays in a natural hyperbolic material. *Nature Communications*, 6(1):6963, apr 2015. ISSN 2041-1723. doi:10.1038/ncomms7963. URL <https://www.nature.com/articles/ncomms7963>.
- [29] Joshua D. Caldwell, Andrey V. Kretinin, Yiguo Chen, Vincenzo Giannini, Michael M. Fogler, Yan Francescato, Chase T. Ellis, Joseph G. Tischler, Colin R. Woods, Alexander J. Giles, Minghui Hong, Kenji Watanabe, Takashi Taniguchi, Stefan A. Maier, and Kostya S. Novoselov. Sub-diffractive volume-confined polaritons in the natural hyperbolic material hexagonal boron nitride. *Nature Communications*, 5(1):5221, oct 2014. ISSN 2041-1723. doi:10.1038/ncomms6221. URL <https://www.nature.com/articles/ncomms6221>.
- [30] Alexander J. Giles, Siyuan Dai, Igor Vurgaftman, Timothy Hoffman, Song Liu, Lucas Lindsay, Chase T. Ellis, Nathanael Assefa, Ioannis Chatzakis, Thomas L. Reinecke, Joseph G. Tischler, Michael M. Fogler, J. H. Edgar, Dimitri N. Basov, and Joshua D. Caldwell. Ultralow-loss polaritons in isotopically pure boron nitride. *Nature Materials*, 17(2):134–139, feb 2018. ISSN 1476-1122. doi:10.1038/nmat5047. URL <http://www.nature.com/articles/nmat5047>.
- [31] Victor W. Brar, Min Seok Jang, Michelle Sherrott, Josue J. Lopez, and Harry A. Atwater. Highly Confined Tunable Mid-Infrared Plasmonics in Graphene Nanoresonators. *Nano Letters*, 13(6):2541–2547, jun 2013. ISSN 1530-6984. doi:10.1021/nl400601c. URL <https://pubs.acs.org/doi/10.1021/nl400601c>.
- [32] Lili Sun, Hao Zhang, Guohua Dong, Ping Li, Zheng Zhu, Yuxiang Li, Chunying Guan, and Jinhui Shi. Dynamically tunable terahertz anomalous refraction and reflection based on graphene metasurfaces. *Optics Communications*, 446:10–15, sep 2019. ISSN 00304018. doi:10.1016/j.optcom.2019.04.058. URL <https://linkinghub.elsevier.com/retrieve/pii/S0030401819303505>.
- [33] Yuancheng Fan, Nian-Hai Shen, Fuli Zhang, Qian Zhao, Zeyong Wei, Peng Zhang, Jiajia Dong, Qunhong Fu, Hongqiang Li, and Costas M. Soukoulis. Photoexcited Graphene Metasurfaces: Significantly Enhanced and Tunable Magnetic Resonances. *ACS Photonics*, 5(4):1612–1618, apr 2018. ISSN 2330-4022. doi:10.1021/acsp Photonics.8b00057. URL <https://pubs.acs.org/doi/10.1021/acsp Photonics.8b00057>.
- [34] Daniel Rodrigo, Tony Low, Damon B Farmer, Hatice Altug, and Phaeton Avouris. Plasmon coupling in extended structures: Graphene superlattice nanoribbon arrays. *Physical Review B*, 93(12):125407, oct 2016. doi:10.1103/physrevb.93.125407. URL <http://arxiv.org/abs/1510.04216><http://dx.doi.org/10.1103/PhysRevB.93.125407>.
- [35] Min Seok Jang, Victor W. Brar, Michelle C. Sherrott, Josue J. Lopez, Laura Kim, Seyoon Kim, Mansoo Choi, and Harry A. Atwater. Tunable large resonant absorption in a midinfrared graphene salisbury screen. *Physical Review B*, 90(16):165409, oct 2014. doi:10.1103/physrevb.90.165409.
- [36] Hugen Yan, Xuesong Li, Bhupesh Chandra, George Tulevski, Yanqing Wu, Marcus Freitag, Wenjuan Zhu, Phaeton Avouris, and Fengnian Xia. Tunable infrared plasmonic devices using graphene/insulator stacks. *Nature Nanotechnology*, 7(April):330–334, apr 2012. ISSN 1748-3387. doi:10.1038/nnano.2012.59. URL <http://www.nature.com/doi/10.1038/nnano.2012.59>.
- [37] Zheyu Fang, Sukosin Thongrattanasiri, Andrea Schlather, Zheng Liu, Lulu Ma, Yumin Wang, Pulickel M. Ajayan, Peter Nordlander, Naomi J. Halas, and F. Javier García de Abajo. Gated Tunability and Hybridization of Localized Plasmons in Nanostructured Graphene. *ACS Nano*, 7(3):2388–2395, mar 2013. ISSN 1936-0851. doi:10.1021/nn3055835. URL <https://pubs.acs.org/doi/10.1021/nn3055835>.
- [38] Weilu Gao, Gang Shi, Zehua Jin, Jie Shu, Qi Zhang, Robert Vajtai, Pulickel M. Ajayan, Junichiro Kono, and Qianfan Xu. Excitation and Active Control of Propagating Surface Plasmon Polaritons in Graphene. *Nano Letters*, 13(8):3698–3702, aug 2013. ISSN 1530-6984. doi:10.1021/nl401591k. URL <https://pubs.acs.org/doi/10.1021/nl401591k>.
- [39] Ci Song, Xiushan Xia, Zheng-Da Hu, Youjian Liang, and Jicheng Wang. Characteristics of Plasmonic Bragg Reflectors with Graphene-Based Silicon Grating. *Nanoscale Research Letters*, 11(1):419, dec 2016. ISSN 1931-

7573. doi:10.1186/s11671-016-1633-0. URL <http://nanoscalereslett.springeropen.com/articles/10.1186/s11671-016-1633-0>.
- [40] Jingchao Song, Lei Zhang, Yunzhou Xue, Qing Yang Steve Wu, Fang Xia, Chao Zhang, Yu-Lin Zhong, Yupeng Zhang, Jinghua Teng, Malin Premaratne, Cheng-Wei Qiu, and Qiaoliang Bao. Efficient Excitation of Multiple Plasmonic Modes on Three-Dimensional Graphene: An Unexplored Dimension. *ACS Photonics*, 3(10):1986–1992, oct 2016. doi:10.1021/acsp Photonics.6b00566. URL <http://dx.doi.org/10.1021/acsp Photonics.6b00566> <http://pubs.acs.org/doi/full/10.1021/acsp Photonics.6b00566>.
- [41] Qinglu Qian, Youjian Liang, Yue Liang, Hongyan Shao, Menglai Zhang, Ting Xiao, and Jicheng Wang. Tunable Multiple-Step Plasmonic Bragg Reflectors with Graphene-Based Modulated Grating. *Sensors*, 16(12):2039, December 2016. ISSN 1424-8220. doi:10.3390/s16122039. URL <http://www.mdpi.com/1424-8220/16/12/2039>.
- [42] Anjali Yadav, Rashmi Kumari, Shailendra K Varshney, and Basudev Lahiri. Tunable phonon-plasmon hybridization in  $\alpha$ -moo3-graphene based van der waals heterostructures. *Optics Express*, 29(21):33171, September 2021. ISSN 1094-4087. doi:10.1364/OE.434993.
- [43] Hodjat Hajian, Amir Ghobadi, Andriy E. Serebryannikov, Bayram Butun, Guy A. E. Vandenbosch, and Ekmel Ozbay. Tunable infrared asymmetric light transmission and absorption via graphene-hbn metamaterials. *Journal of Applied Physics*, 126(19):193102, November 2019. ISSN 1089-7550. doi:10.1063/1.5118887.
- [44] V. V. Popov, T. Yu. Bagaeva, T. Otsuji, and V. Ryzhii. Oblique terahertz plasmons in graphene nanoribbon arrays. *Physical Review B*, 81(7):073404, feb 2010. ISSN 1098-0121. doi:10.1103/PhysRevB.81.073404. URL <https://link.aps.org/doi/10.1103/PhysRevB.81.073404>.
- [45] Long Ju, Baisong Geng, Jason Horng, Caglar Girit, Michael Martin, Zhao Hao, Hans a. Bechtel, Xiaogan Liang, Alex Zettl, Y Ron Shen, and Feng Wang. Graphene plasmonics for tunable terahertz metamaterials. *Nature Nanotechnology*, 6(10):630–634, oct 2011. ISSN 1748-3387. doi:10.1038/nnano.2011.146. URL <http://www.nature.com/doifinder/10.1038/nnano.2011.146> <http://www.ncbi.nlm.nih.gov/pubmed/21892164> <http://www.nature.com/articles/nnano.2011.146>.
- [46] F. Hu, Y. Luan, Z. Fei, I. Z. Palubski, M. D. Goldflam, S. Dai, J.-S. Wu, K. W. Post, G. C. A. M. Janssen, M. M. Fogler, and D. N. Basov. Imaging the Localized Plasmon Resonance Modes in Graphene Nanoribbons. *Nano Letters*, 17(9):5423–5428, sep 2017. ISSN 1530-6984. doi:10.1021/acs.nanolett.7b02029. URL <https://pubs.acs.org/doi/10.1021/acs.nanolett.7b02029>.
- [47] Hugen Yan, Tony Low, Wenjuan Zhu, Yanqing Wu, Marcus Freitag, Xuesong Li, Francisco Guinea, Phaedon Avouris, and Fengnian Xia. Damping pathways of mid-infrared plasmons in graphene nanostructures. *Nature Photonics*, 7(5):394–399, may 2013. ISSN 1749-4885. doi:10.1038/nphoton.2013.57. URL <http://www.nature.com/articles/nphoton.2013.57>.
- [48] Marcus Freitag, Tony Low, Wenjuan Zhu, Hugen Yan, Fengnian Xia, and Phaedon Avouris. Photocurrent in graphene harnessed by tunable intrinsic plasmons. *Nature Communications*, 4(1):1951, jun 2013. ISSN 2041-1723. doi:10.1038/ncomms2951. URL <https://www.nature.com/articles/ncomms2951>.
- [49] Christian Sorger, Sascha Preu, Johannes Schmidt, Stephan Winnerl, Yuliy V Bludov, Nuno M R Peres, Mikhail I Vasilevskiy, and Heiko B Weber. Terahertz response of patterned epitaxial graphene. *New Journal of Physics*, 17(5):053045, may 2015. ISSN 1367-2630. doi:10.1088/1367-2630/17/5/053045. URL <http://stacks.iop.org/1367-2630/17/i=5/a=053045?key=crossref.97ba9a16f5ff535e572eded19ae8d644>.
- [50] Hong-Son Chu and Choon How Gan. Active plasmonic switching at mid-infrared wavelengths with graphene ribbon arrays. *Applied Physics Letters*, 102(23):231107, jun 2013. doi:10.1063/1.4810003.
- [51] P. A. D. Gonçalves, E. J. C. Dias, Yu. V. Bludov, and N. M. R. Peres. Modeling the excitation of graphene plasmons in periodic grids of graphene ribbons: An analytical approach. *Physical Review B*, 94(19):195421, nov 2016. ISSN 2469-9950. doi:10.1103/PhysRevB.94.195421. URL <http://link.aps.org/doi/10.1103/PhysRevB.94.195421>.
- [52] Mahdi Rahmanzadeh, Ali Abdolali, Amin Khavasi, and Hamid Rajabalipanah. Adopting image theorem for rigorous analysis of a perfect electric conductor-backed array of graphene ribbons. *Journal of the Optical Society of America B*, 35(8):1836, August 2018. ISSN 0740-3224, 1520-8540. doi:10.1364/JOSAB.35.001836. URL <https://opg.optica.org/abstract.cfm?URI=josab-35-8-1836>.
- [53] Tatiana L Zinenko. Scattering and absorption of terahertz waves by a free-standing infinite grating of graphene strips: analytical regularization analysis. *Journal of Optics*, 17(5):055604, apr 2015. doi:10.1088/2040-8978/17/5/055604.

- [54] Borislav Vasić, Goran Isić, and Radoš Gajić. Localized surface plasmon resonances in graphene ribbon arrays for sensing of dielectric environment at infrared frequencies. *Journal of Applied Physics*, 113(1):013110, jan 2013. doi:10.1063/1.4773474.
- [55] Ruey-Bing Hwang. A theoretical design of evanescent wave biosensors based on gate-controlled graphene surface plasmon resonance. *Scientific Reports*, 11(1):1999, jan 2021. ISSN 2045-2322. doi:10.1038/s41598-021-81595-9. URL <https://doi.org/10.1038/s41598-021-81595-9><https://www.nature.com/articles/s41598-021-81595-9>.
- [56] Nestor Jr. Bareza, Ewelina Wajs, Bruno Paulillo, Antti Tullila, Hannakaisa Jaatinen, Roberto Milani, Camilla Dore, Agustin Mihi, Tarja K. Nevanen, and Valerio Pruneri. Quantitative mid-infrared plasmonic biosensing on scalable graphene nanostructures. *Advanced Materials Interfaces*, 10(2):2201699, January 2023. ISSN 2196-7350, 2196-7350. doi:10.1002/admi.202201699. URL <https://onlinelibrary.wiley.com/doi/10.1002/admi.202201699>.
- [57] Jinpeng Nong, Wei Wei, Guilian Lan, Peng Luo, Caicheng Guo, Juemin Yi, and Linlong Tang. Resolved infrared spectroscopy of aqueous molecules employing tunable graphene plasmons in an otto prism. *Analytical Chemistry*, 92(23):15370–15378, sep 2020. doi:10.1021/acs.analchem.0c02733.
- [58] Hai Hu, Xiaoxia Yang, Xiangdong Guo, Kaveh Khaliji, Sudipta Romen Biswas, F. Javier García de Abajo, Tony Low, Zhipei Sun, and Qing Dai. Gas identification with graphene plasmons. *Nature Communications*, 10(1):1131, mar 2019. ISSN 2041-1723. doi:10.1038/s41467-019-09008-0. URL <https://www.nature.com/articles/s41467-019-09008-0>.
- [59] Damon B. Farmer, Phaedon Avouris, Yilei Li, Tony F. Heinz, and Shu-Jen Han. Ultrasensitive plasmonic detection of molecules with graphene. *ACS Photonics*, 3(4):553–557, apr 2016. doi:10.1021/acsp Photonics.6b00143.
- [60] Yilei Li, Huguen Yan, Damon B. Farmer, Xiang Meng, Wenjuan Zhu, Richard M. Osgood, Tony F. Heinz, and Phaedon Avouris. Graphene plasmon enhanced vibrational sensing of surface-adsorbed layers. *Nano Letters*, 14(3):1573–1577, feb 2014. doi:10.1021/nl404824w.
- [61] Hai Hu, Xiangdong Guo, Debo Hu, Zhipei Sun, Xiaoxia Yang, and Qing Dai. Flexible and Electrically Tunable Plasmons in Graphene-Mica Heterostructures. *Advanced Science*, 5(8):1800175, August 2018. ISSN 21983844. doi:10.1002/advs.201800175. URL <https://onlinelibrary.wiley.com/doi/10.1002/advs.201800175>.
- [62] Daniel Rodrigo, Odeta Limaj, Davide Janner, Dordaneh Etezadi, F. Javier García De Abajo, Valerio Pruneri, and Hatice Altug. Mid-infrared plasmonic biosensing with graphene. *Science*, 349(6244):165–168, 2015. ISSN 10959203. doi:10.1126/science.aab2051.
- [63] Jun Wu, Changhe Zhou, Junjie Yu, Hongchao Cao, Shubin Li, and Wei Jia. Design of infrared surface plasmon resonance sensors based on graphene ribbon arrays. *Optics & Laser Technology*, 59:99–103, jul 2014. doi:10.1016/j.optlastec.2013.12.019.
- [64] Hai Hu, Xiaoxia Yang, Feng Zhai, Debo Hu, Ruina Liu, Kaihui Liu, Zhipei Sun, and Qing Dai. Far-field nanoscale infrared spectroscopy of vibrational fingerprints of molecules with graphene plasmons. *Nature Communications*, 7(1), July 2016. ISSN 2041-1723. doi:10.1038/ncomms12334.
- [65] André Souto, Diogo Cunha, and Mikhail I. Vasilevskiy. Modeling of a plasmonic biosensor based on a graphene nanoribbon superlattice. *physica status solidi (b)*, 259(11), March 2022. ISSN 1521-3951. doi:10.1002/pssb.202200055.
- [66] Xianglong Miao, Lingyue Yan, Yun Wu, and Peter Q. Liu. High-sensitivity nanophotonic sensors with passive trapping of analyte molecules in hot spots. *Light: Science & Applications*, 10(1), January 2021. ISSN 2047-7538. doi:10.1038/s41377-020-00449-7.
- [67] Nestor Jr. Bareza, Bruno Paulillo, Tetiana M. Slipchenko, Marta Autore, Irene Dolado, Song Liu, James H. Edgar, Saül Vélez, Luis Martín-Moreno, Rainer Hillenbrand, and Valerio Pruneri. Phonon-enhanced mid-infrared CO<sub>2</sub> gas sensing using boron nitride nanoresonators. *ACS Photonics*, 9(1):34–42, January 2022. ISSN 2330-4022. doi:10.1021/acsp Photonics.1c01254.
- [68] Anjali Yadav, Shailendra K. Varshney, and Basudev Lahiri. Hybridized phonon polaritons assisted broad range seira-based multimolecular sensing. *IEEE Sensors Journal*, 23(18):21812–21820, September 2023. ISSN 2379-9153. doi:10.1109/JSEN.2023.3299447.
- [69] Anshuman Kumar, Tony Low, Kin Hung Fung, Phaedon Avouris, and Nicholas X. Fang. Tunable Light-Matter Interaction and the Role of Hyperbolicity in Graphene-hBN System. *Nano Letters*, 15(5):3172–3180, may 2015. ISSN 1530-6984. doi:10.1021/acs.nanolett.5b01191. URL <http://dx.doi.org/10.1021/acs.nanolett.5b01191><http://pubs.acs.org/doi/abs/10.1021/acs.nanolett.5b01191>.

- [70] Yu V Bludov, N M R Peres, and M I Vasilevskiy. Unusual reflection of electromagnetic radiation from a stack of graphene layers at oblique incidence. *Journal of Optics*, 15(11):114004, oct 2013. doi:10.1088/2040-8978/15/11/114004.
- [71] Yongjiao Wen, Yu Sun, Chunyu Deng, Lei Huang, Guohua Hu, Binfeng Yun, Ruohu Zhang, and Yiping Cui. High sensitivity and FOM refractive index sensing based on fano resonance in all-grating racetrack resonators. *Optics Communications*, 446:141–146, sep 2019. doi:10.1016/j.optcom.2019.04.068.
- [72] Qing-Qing Meng, Xin Zhao, Cheng-You Lin, Shu-Jing Chen, Ying-Chun Ding, and Zhao-Yang Chen. Figure of merit enhancement of a surface plasmon resonance sensor using a low-refractive-index porous silica film. *Sensors*, 17(8):1846, aug 2017. doi:10.3390/s17081846.
- [73] AmirHossein Norouzi Razani, Pejman Rezaei, Pouria Zamzam, Seyed Amin Khatami, and Omid Mohsen Daraei. Absorption-based ultra-sensitive ri sensor based on the flower-shaped graphene resonator for early detection of cancer. *Optics Communications*, 524:128775, December 2022. ISSN 0030-4018. doi:10.1016/j.optcom.2022.128775.
- [74] Tao Chen, Dapeng Zhang, Fengyu Huang, Zhi Li, and Fangrong Hu. Design of a terahertz metamaterial sensor based on split ring resonator nested square ring resonator. *Materials Research Express*, 7(9):095802, September 2020. ISSN 2053-1591. doi:10.1088/2053-1591/abb496.
- [75] Zhimin Liu, Shanshan Zhuo, Fengqi Zhou, Xiao Zhang, Yipeng Qin, Xin Luo, Cheng Ji, and Guangxin Yang. Double narrowband induced perfect absorption photonic sensor based on graphene–dielectric–gold hybrid metamaterial. *Nanoscale Research Letters*, 17(1), September 2022. ISSN 1556-276X. doi:10.1186/s11671-022-03724-1.
- [76] Saeedeh Barzegar-Parizi. Refractive index sensor with dual sensing bands based on array of jerusalem cross cavities to detect the hemoglobin concentrations. *Optical and Quantum Electronics*, 55(1), December 2022. ISSN 1572-817X. doi:10.1007/s11082-022-04296-1.
- [77] Sebastián Castilla, Ioannis Vangelidis, Varun-Varma Pusapati, Jordan Goldstein, Marta Autore, Tetiana Slipchenko, Khannan Rajendran, Seyoon Kim, Kenji Watanabe, Takashi Taniguchi, Luis Martín-Moreno, Dirk Englund, Klaas-Jan Tielrooij, Rainer Hillenbrand, Eleftherios Lidorikis, and Frank H. L. Koppens. Plasmonic antenna coupling to hyperbolic phonon-polaritons for sensitive and fast mid-infrared photodetection with graphene. *Nature Communications*, 11(1), September 2020. ISSN 2041-1723. doi:10.1038/s41467-020-18544-z.
- [78] Achim Woessner, Romain Parret, Diana Davydovskaya, Yuanda Gao, Jih-Sheng Wu, Mark B. Lundeberg, Sébastien Nanot, Pablo Alonso-González, Kenji Watanabe, Takashi Taniguchi, Rainer Hillenbrand, Michael M. Fogler, James Hone, and Frank H. L. Koppens. Electrical detection of hyperbolic phonon-polaritons in heterostructures of graphene and boron nitride. *npj 2D Materials and Applications*, 1(1), August 2017. ISSN 2397-7132. doi:10.1038/s41699-017-0031-5.

## 6 Hyperbolic phonon-plasmon polaritons in a hBN-graphene van der Waals structure: supplemental document

### 6.1 Spatial distributions of electric field of diffracted wave

Figure 9 shows spatial distributions of  $x$ -component of the electric field over one period of the periodic structure (horizontal  $x$ -axis) at frequencies, corresponding to absorbance maxima in Figure 4 of main text. For the absorbance maximum nearby  $\lambda = 5.85 \mu\text{m}$  electric field distribution [Figure 9(a)] is characterized by the minimum in the vicinity of the graphene strip (green horizontal lines) and maximum beyond the graphene (notice that after half-period of temporal oscillations  $T = \lambda/(2c)$ , where  $c$  is the speed of light, these minima and maxima will be inverted). The distribution of electric field along  $z$ -axis [Figure 9(b)], taken at the center of graphene strip  $x = 0$  demonstrates the maximum of field’s absolute value in the vicinity of graphene, thus resembling the eigenmode distribution of Figure 2(e) of main text (plasmonic-like mode). The last fact allows to conclude, that enhanced absorbance happens due to the excitation of plasmonic-like mode.

The field distribution, which corresponds to the absorbance maximum  $\lambda = 6.725 \mu\text{m}$  is characterized by the low field in the vicinity of graphene [see Figure 9(c)]. At the same time, electric field distribution along  $z$ -axis [Figure 9(d)] shows one sign variation, which resembles the mode, depicted in Figure 2(f) (waveguide-like mode in upper restrahlen band) of the main text.

The field distribution, corresponding to absorbance maxima nearby  $\lambda = 9.24 \mu\text{m}$  (between restrahlen bands), shown in Figures 9(e) and 9(f) is similar to those of absorbance maximum nearby  $\lambda = 5.85 \mu\text{m}$  [Figures 9(a) and 9(b)], except higher degree of localization of field in the vicinity of graphene for plasmonic-like mode at  $\lambda = 9.24 \mu\text{m}$ .

Electric field distributions, corresponding to absorbance maxima  $\lambda = 12.2 \mu\text{m}$  and  $\lambda = 12.285 \mu\text{m}$  [depicted in Figures 9(g), 9(h) and Figures 9(i), 9(j), respectively] resemble waveguide-like modes in lower restrahlen band, shown in Figures 3(f) and 3(e) of the main text. The situation is more complicated for the field distribution, corresponding to absorbance maximum at  $\lambda = 12.86 \mu\text{m}$ , where field maxima are arranged nearby edges of hBN film [see Figure 9(k)]. Except the fact, that absorbance maxima is located beyond the restrahlen bands, the field distribution along  $z$ -axis, shown in Figure 9(l) is not similar to the plasmonic-like mode, shown in Figure 3(i) of the main text.

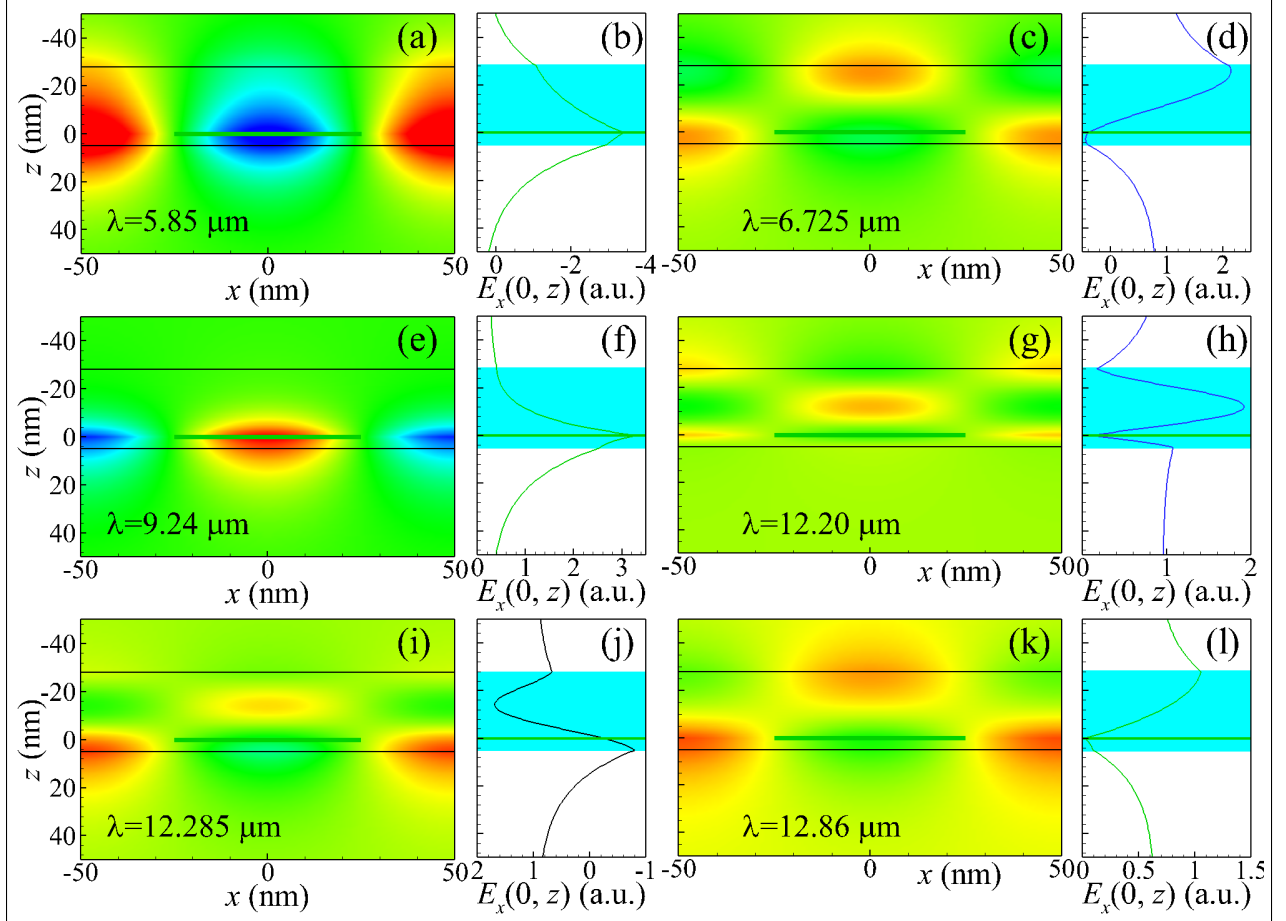


Figure 9: Spatial distributions of in-plane component of electric field  $E_x(x, z)$  [panels (a), (c), (e), (g), (i), (k)] and the same dependencies at the graphene center  $E_x(0, z)$  [panels (b), (d), (f), (h), (j), (l)] at vacuum wavelengths  $\lambda = 5.85 \mu\text{m}$  [panels (a) and (b)],  $\lambda = 6.725 \mu\text{m}$  [panels (c) and (d)],  $\lambda = 9.24 \mu\text{m}$  [panels (e) and (f)],  $\lambda = 12.2 \mu\text{m}$  [panels (g) and (h)],  $\lambda = 12.285 \mu\text{m}$  [panels (i) and (j)], and  $\lambda = 12.86 \mu\text{m}$  [panels (k) and (l)]. Other parameters are the same, as in Fig. 4 of the main text. In all panels position of graphene strips are depicted by green lines.